Improvement of 1D geoelectric sounding by narrowing the equivalence range and identification, quantification and reduction of lateral effects using the tri-potential technique

Filip Arnaut [ORCID]*, Branislav Sretenović and Vesna Cvetkov* [ORCID]

Department of Geophysics, Faculty of Mining and Geology, University of Belgrade, Belgrade, Serbia

Apparent resistivity data from the Offset-Wenner array (Zemun, Serbia), the square array (Bogatić and Golubac, Serbia) and the Wenner tri-potential technique (Vrdnik, Serbia), were used to detect, measure, and reduce lateral effects in 1D inversion. Forward and inverse modelling with the Wenner α, ß and γ arrays determined that the Wenner ß array provided the most accurate estimate of the first-and second-layer resistivity, while the Wenner γ array provided the most accurate estimate of the high resistivity substratum. The survey on the Zemun loess plateau revealed that if the lateral index of inhomogeneity (*LII*) is low, the 1D interpretation of both Wenner arrays is justifiable. In addition, the averaging of resistances will result in an apparent resistivity curve that is devoid of lateral effects resulting from near-surface inhomogeneities. As demonstrated by the Vrdnik example, 1D inversion is inadequate when the values of *LII* and processing covariance (*PC*) are high. The survey in Golubac was conducted using the square array, which produced lower *PC* values than collinear arrays. Therefore, the quality of the averaged sounding curve was higher. Also, the interpolated values of the Offset Wenner array displayed reasonable accuracy, while the extrapolated values were inadequate when a low resistivity substratum was present.

Keywords: near-surface, 2D electrical resistivity tomography, inversion, Offset Wenner array, square array, effect of near-surface inhomogeneities on 1D measurements.

Introduction

The tri-potential technique was developed in the mid-twentieth century (Carpenter, 1955; Carpenter and Habberjam, 1956; Habberjam, 1969). However, it was never widely used because it required additional measurements that made this technique less effective

in comparison with traditional resistivity survey techniques. Improvements in data acquisition, which began in the late 1980s, made this technique more effective, and the additional data that this technique provides made it useful for 1D, 2D, and 3D interpretations in terms of lateral effects detection, quantification, and reduction, as well as reducing the number of subsurface equivalent models.

Simultaneous measurements of lateral and vertical resistivity changes using the tri-potential technique are now a part of modern 2D survey methods (electrical resistivity tomography – ERT). However, this type of measurement has not found widespread use in 1D vertical electrical sounding (VES). The additional data obtained by the tri-potential technique enable the detection, quantification, and reduction of lateral effects (Habberjam and Watkins, 1967a), as well as the improvement of the overall measurement accuracy using the relationship between the three measured resistivities ($\rho_a{}^\alpha$, $\rho_a{}^\beta$, $\rho_a{}^\gamma$).

In the 1D model case, where resistivity changes with depth only, the sounding curves $\rho_a{}^\alpha$, $\rho_a{}^\beta$, and $\rho_a{}^\gamma$ will exhibit the same general pattern. However, at different depths of investigation, changes in resistivity will be observed first on the $\rho_a{}^\gamma$ sounding curve and lastly on the $\rho_a{}^\beta$ sounding curve *i.e.*, the (Wenner) gamma array displays the greatest depth of investigation values (Szalai et al., 2014; Loke, 2022). In the case of resistivity increase with depth, the $\rho_a{}^\gamma$ sounding curve will display the highest resistivity values, while the $\rho_a{}^\beta$ sounding curve will show the lowest resistivity values. If the model is inverted (resistivity decrease with depth) the order will be reversed ($\rho_a{}^\gamma < \rho_a{}^\alpha < \rho_a{}^\beta$) (Acworth and Griffits, 1985).

In this study, we use the apparent resistivity data measured by the Offset-Wenner array on the Zemun loess plateau (Serbia), as well as data from the square array (Bogatić and Golubac, Serbia) and the Wenner tri-potential technique (Vrdnik, Serbia). The results of the data processing used to detect, measure, and reduce lateral effects in 1D inversion were studied on the measured data while the lateral effects affecting the 1D, 2D, and 3D inversion were studied on the synthetic models.

2. Methodology

2.1. The Wenner tri-potential resistivity technique

Electrical resistivity measurements are based on the injection of an electric current into the ground by two current electrodes (C_1C_2) and measuring the potential difference by two potential electrodes (P_1P_2) (Carpenter, 1955; Zhou, 2016). The tri-potential technique involves measuring three apparent resistivities (or resistances) using a four-electrode array (Carpenter and Habberjam, 1956). Therefore, measurements with the Wenner tri-potential technique consist of measuring three apparent resistivities ($\rho_a{}^\alpha$, $\rho_a{}^\beta$, $\rho_a{}^\gamma$) with a four-electrode, colinear, equidistant array (Fig. 1a). Measured apparent resistivities are denoted by $\rho_a{}^\alpha$ ($C_1P_1P_2C_2$), $\rho_a{}^\beta$ ($C_1C_2P_1P_2$) and $\rho_a{}^\gamma$ ($C_1P_1C_2P_2$) (Carpenter, 1955; Carpenter and Habberjam, 1956; Acworth and Griffits, 1985).

The percent of lateral effects in a certain segment of the apparent resistivity sounding curve is described as the ratio of lateral inhomogeneity (*LIR*). The interference of lateral effects can be measured for a part of the resistivity sounding curve using a series of *LIR* values. The root mean square of the lateral inhomogeneity ratio is used to measure the index of lateral inhomogeneity (*LII*):
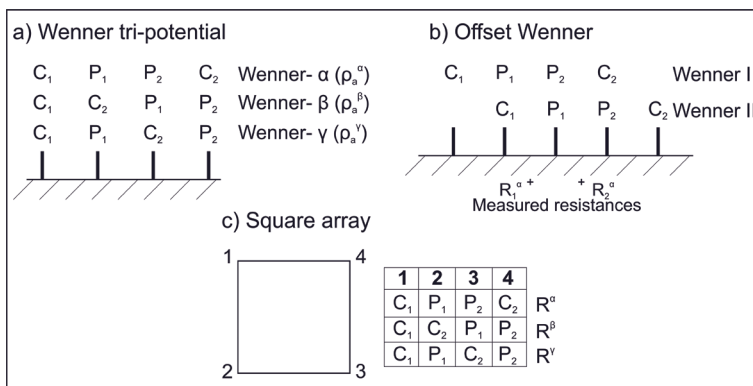
Figure 1. (*a*) The Wenner tri-potential technique; (*b*) The Offset Wenner array; (*c*) The square array.

$$LII=\sqrt{\frac{1}{m}\sum_{i=1}^{m}(LIR)^2}\,, \tag{1}$$

where m is the upper limit of summation. The load of the entire resistivity sounding curve by lateral effects is determined using the index of lateral inhomogeneity. The authors of the study on lateral effects identification, quantification, and reduction suggested criteria for classifying the lateral effects load Habberjam and Watkins (1967a):

  – $0\% \leq LII \leq 20\%$ – good quality sounding curves,
  – $20\% \leq LII \leq 50\%$ – medium quality sounding curves,
  – $LII \geq 50\%$ – bad quality sounding curves.

The processed resistivity sounding curve ($\rho_a{}^o$) is the result of lateral effect reduction, *i.e.*, it is a precise method of adjusting measured apparent resistivities to the nearest 1D model. The processing covariance (*PC*) is used to calculate the deviation of the processed sounding curve $\rho_a{}^o$ from the measured sounding curve $\rho_a{}^m$. Values of processing covariance are higher if the measured sounding curve is influenced by lateral effects. The processing covariance is calculated as:

$$PC=\frac{1}{m}\sum_{i=1}^{m}[(\log \rho_a^m)_i - (\log \rho_a^o)_i]^2, \tag{2}$$

where m is the upper limit of summation. If the value of processing covariance decreases, the results of quantitative 1D inversion become more accurate. Processing covariance values are dependent on measurement precision and local geology, *i.e.*, how much does the local geology deviate from a 1D subsurface model.

2.2. The Offset Wenner array

The Offset-Wenner array (Fig. 1b) was introduced in 1981 by Barker as a five electrode, colinear, non-focused, superposed array (Szalai and Szarka, 2008) consisting of two mutually shifted Wenner arrays (Barker, 1981; White and Scott, 1988). The Offset-

Wenner array consists of two distinct measurements, one with electrodes 1-2-3-4 (Wenner I) and the other with electrodes 2-3-4-5 (Wenner II). Measurement with the Offset-Wenner array can also be done in a tri-potential manner, as it was depicted in Fig. 1a where a total of six resistances can be obtained ($R_1{}^{\alpha}$, $R_2{}^{\alpha}$, $R_1{}^{\beta}$, $R_2{}^{\beta}$, $R_1{}^{\gamma}$, $R_2{}^{\gamma}$). The main advantage the Offset-Wenner array possesses is the detection and elimination of lateral resistivity effects (Barker, 1981; Nunn et al., 1983; Busby and Peart, 1997). The Offset-Wenner array also enables automatization of data acquisition as well as the extrapolation of the calculated apparent resistivity sounding curve (Barker, 1981). Several authors such as White and Scott (1988) and Chermail et al. (2018) considered the accuracy of the calculated interpolated data of the Offset-Wenner sounding curve, which was obtained on distances "a" generated by the relationship for the electrode spreading (S):

$$S = 3 \times 2^n \times a, \, n = 0, 1, 2, 3... \tag{3}$$

and the accuracy of the extrapolated data point, which was obtained for the distance of $2a$ with the respect to the last measured data point "a" (White and Scott, 1988; Chermali et al., 2018).

Electrical resistances $R_1{}^{\alpha}$ and $R_2{}^{\alpha}$ measured with two shifted Wenner arrays (Wenner I and Wenner II) that allow for the detection of near-surface lateral inhomogeneities and subsequent reduction of those effects by averaging $R_1{}^{\alpha}$ and $R_2{}^{\alpha}$. The offset error (E_{of}) is used to calculate lateral effects:

$$E_{of} = \frac{R_1{}^{\alpha} - R_2{}^{\alpha}}{R_1{}^{\alpha}} \tag{4}$$

The electrode spreading (S) is done according to the rule:

$$S = 2^n \times a, n = 0, 1, 2, 3..., \tag{5}$$

with the inner electrode taking the place of the former outer electrode (Fig. 2).

The electrical resistances R_a, R_b, and R_c, which are measured with electrodes 1, 2, 4, and 5, are primarily used to calculate the resistance R_a value at electrode spacing according to the rule:

$$S = 3 \times 2^n \times a, n = 0, 1, 2, 3. \tag{6}$$

Even though the Offset Wenner and the tri-potential Wenner arrays are the most efficient for the reduction of lateral effects (apart from the square array), a limited number of data points on the sounding curve lessen the quality of detection and reduction of lateral effects for the Offset Wenner array.
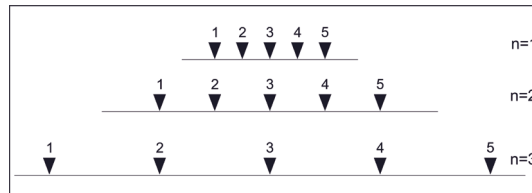

Figure 2. Offset Wenner array resistivity sounding.

2.3. The square array

The square array (Fig. 1c) was first introduced in 1967 as a non-collinear, non-super-posed and non-focused array (Szalai and Szarka, 2008). The primary purpose of the square array was addressing directional dependence of resistivity measurements that arise with conventional collinear and symmetrical arrays such as the Wenner or Schlumberger array (Habberjam and Watkins, 1967a). The square array measurements are done in a tri-potential manner, with resistance measurements taken in two perpendicular directions (R^α, R^β) and a control measurement in the diagonal direction (R^γ). The square array can then be rotated by 45°, and measurements repeated, *i.e.*, the crossed square array. Alternatively, the square array can be expanded by $a\sqrt{2}$ and measurements for a larger electrode spacing can be performed. Apparent resistivities can be obtained from measured resistances by simple equations given in Habberjam and Watkins (1967b).

Averaging the $\rho_a{}^\alpha$ and $\rho_a{}^\beta$ sounding curves, which were determined by the square array, Habberjam and Watkins (1967b) established a numerical method for reducing lateral effects.

In the case of a 1D subsurface model, the apparent resistivities measured in two perpendicular directions are identical (in fact, they vary with the value of the measurement error). Only the presence of inhomogeneities causes the two sounding curves to diverge. Such divergences are calculated for each data point in the sounding curve using a simple equation for azimuthal inhomogeneity ratio (*AIR*). The azimuthal inhomogeneity index is calculated by taking the root-mean-square value from the azimuthal inhomogeneity ratio:

$$AIR(a) = \frac{2R^\gamma(a)}{R^\alpha(a) + R^\beta(a)}, \tag{7}$$

$$AII(a) = \sqrt{\frac{1}{m}\sum_{i=1}^{m}(AIR)^2}, \tag{8}$$

where m is the upper limit of summation.

3. Results and discussion

3.1. Model equivalence analysis with the Wenner tri-potential technique

For two geoelectric sections, it can be said to be equivalent when the result of layering produces two practically identical sounding curves (Zohdy, 1949; Bhatacharrya and Shalivahan, 2016). For example, two H-type curves can be equivalent (with respect to the longitudinal conductivity – S) if the middle layer has a small thickness and resistivity compared to the other two adjacent layers (Bhatacharrya and Parta, 1968; Sanuade et al., 2019).

The magnitude of the minima of the sounding curves $\rho_a{}^\alpha$, $\rho_a{}^\beta$ and $\rho_a{}^\gamma$ vary due to different depths of investigation (Acworth and Griffits,1985). The 1D inversion of the $\rho_a{}^\beta$ sounding curve will determine the best true resistivity value of the middle layer, which is critical for a correct definition of the thickness of the second layer according to the principle of equivalence. For the 1D, 2D, and 3D geoelectrical surveys, the equivalence principle applies. The ambiguity of the inversion results increases when the thickness of the second layer is smaller than the thickness of the first (surface) layer.

Figure 3a demonstrates a case where the second layer resistivity is modified by 50% using the equivalence principle for contrast resistivities $\rho_2/\rho_3 \geq 10$ (Maillet, 1947; Koefoed, 1969), and the thickness h_2 changes linearly to 22.5 m (that is equivalent to the increase of 50% as well). In the presence of a thin layer ($h_2 \leq h_1$), and/or when the layer thicknesses in the model do not increase progressively with depth, the range of equivalence can be very broad.

To analyze the range of equivalence for the 1D model from Acworth and Griffits (1985), sections of apparent resistivity for the Wenner α, β, and γ arrays were calculated, the dataset was then used in the 2D inversion. Figure 3b displays the 1D model from Acworth and Griffits (1985) and the apparent resistivity section for the Wenner α (Fig. 3c) and β array (Fig. 3d).
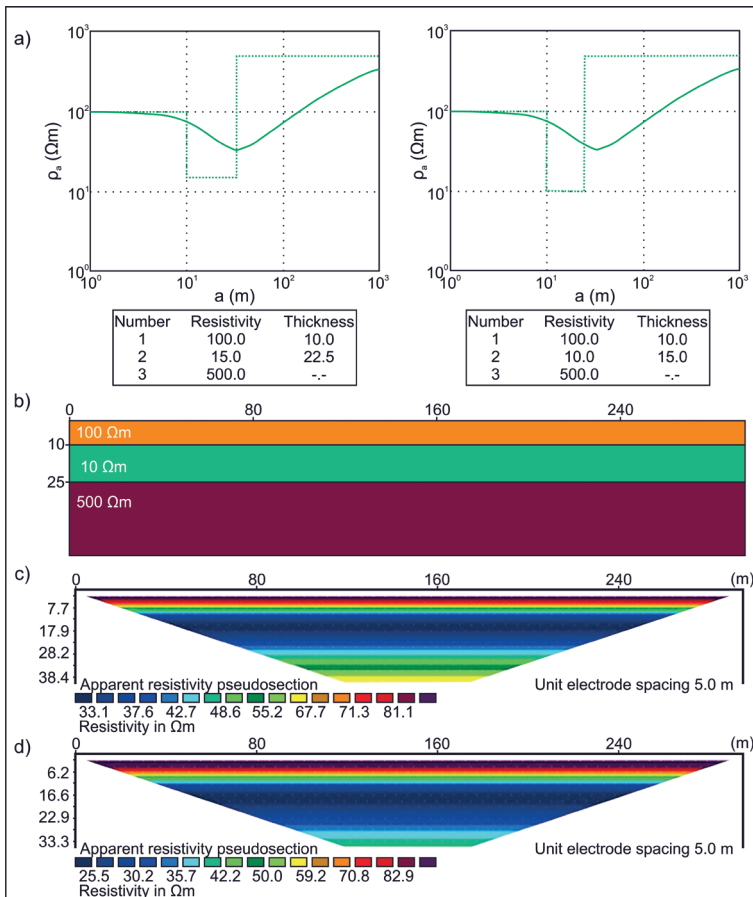

Figure 3. (*a*) Equivalent models obtained by the 1D inversion of the sounding curve from Acworth and Griffits (1985); (*b*) 1D subsurface model from Acworth and Griffits (1985); (*c*) apparent resistivity section for the Wenner α array; (*d*) apparent resistivity section for the Wenner β array; ρ_a – apparent resistivity.

The apparent resistivity section from Fig. 3c indicates that the minimal resistivity value is 33 Ωm. This is confirmed with the minimal resistivity from the Wenner α sounding curve from Acworth and Griffits (1985). The minimum apparent resistivity value of 25.5 Ωm can be seen in the apparent resistivity section measured with the Wenner β array for the same subsurface model. The lower resistivity value is due to the Wenner-β array's lower depth of investigation (Edwards, 1977; Loke, 2022), thus the measured apparent resistivities are more affected by the second low resistivity layer (10 Ωm).

The apparent resistivity pseudosections (Figs. 3c and 3d) were utilized for 2D inversion with a total of three iterations for *RMS* convergence. The results of 2D inversion obtained by Wenner α, β, and γ arrays (Fig. 4) confirm that inversion of the Wenner-β array yields the best true resistivity value and thickness of the second layer. The Wenner-γ array is the most fitting method for evaluating the true resistivity value of the substratum.

The previous example used the resistivity model from Acworth and Griffits (1985), but the thickness of the first and second layers was altered to obtain additional information about the capabilities of the Wenner α, β and γ arrays and to conduct statistical analysis (Tab. 1). The initial model (M1) consisted of a 100 Ωm first layer with a 5 m relative thickness, while the second, low resistivity (10 Ωm) layer had a 20 m thickness. In each instance, the resistivity of the substratum remained the same (500 Ωm). Each model after the initial model (M1) had increased thickness of the first layer by 2.5 m and decreased thickness of the second layer by 2.5 m. Seven models were constructed in total.

Each model was constructed using the RES2DMOD forward modelling software (Loke, 2016) with 60 electrodes total, a unit electrode spacing of 5 m, and four nodes per
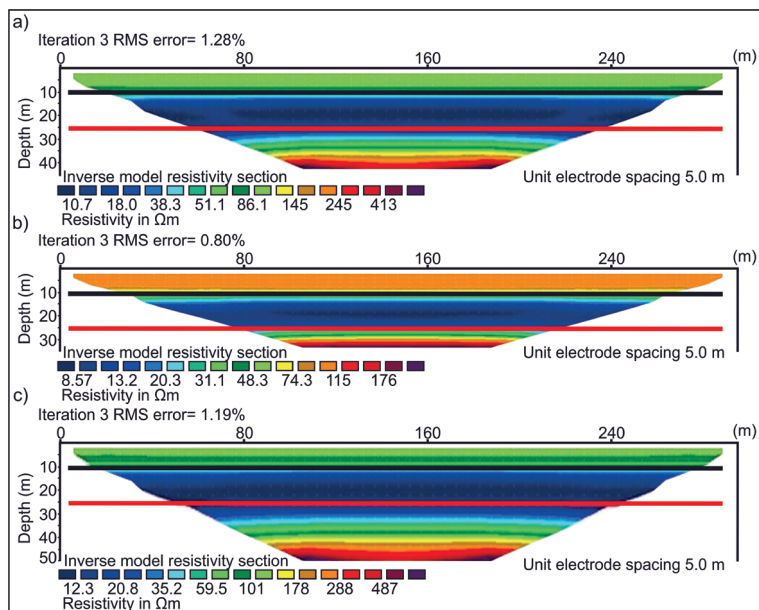

Figure 4. Results of 2D inversion for (*a*) Wenner α; (*b*) Wenner β; (*c*) Wenner γ array. Red line – the true depth to the high resistivity substratum; black line – the depth to the second layer.

Table 1. Forward model parameters for the statistical analysis of Wenner α, β and γ arrays based on the model given in Ackworth and Griffits (1985); h_1 and h_2 – thickness of the first and layer; ρ_1, ρ_2 and ρ_3 – resistivities of the first, second and third layer.

Model name	Model parameters				
	h_1 [m]	ρ_1 [Ωm]	h_2 [m]	ρ_2 [Ωm]	ρ_3 [Ωm]
M1	5	100	20	10	500
M2	7.5	100	17.5	10	500
M3	10	100	15	10	500
M4	12.5	100	12.5	10	500
M5	15	100	10	10	500
M6	17.5	100	7.5	10	500
M7	20	100	5	10	500

electrode spacing. In the first 30 meters of the forward model, the horizontal and vertical dimensions of the mesh cells were 2.5 m. After the 30th meter, the dimensions of the cells were generated automatically. To simulate real measurements, random noise of ±2% was added to each individual model after forward modeling. The least squares inversion parameters in RES2DINV (Loke, 1994) software for each model were constant. The maximum number of iterations for the RMS convergence were increased to five with the standard Gauss-Newton was the optimization method. The models obtained after inversion were exported to Surfer (Golden Software), thus allowing for additional statistical analysis. The data corresponding to the first, second, and third layers of the forward model were extracted from the model obtained after inversion and analyzed.

Table 2 provides a brief statistical summary of the minimum, maximum, and mean apparent resistivity of the Wenner α, β and γ arrays for all three layers of the seven models. To estimate the accuracy of the resistivity measurements for the three Wenner arrays, the absolute error (*ABSE*) was calculated using the difference between the calculated mean after inversion and the true resistivity of a given layer.

For the first layer, the Wenner β array has, on average, the smallest absolute error with a value of 5.51 Ωm, followed by the Wenner α array with 6.85 Ωm and then the Wenner γ array with 8.11 Ωm. In addition, the Wenner γ array displays (on average) the lowest mean resistivity value for the first layer with 93.32 Ωm, followed by the Wenner α array with 94.46 Ωm and the Wenner α array with 96.02 Ωm. Since we are aware that the second layer has a low resistivity, the values of the mean resistivity for the three arrays correspond well with the median depth of investigation for the three arrays that is given in Loke (2022). The array with the greatest resistivity corresponds to the Wenner β with the smallest depth of investigation, and vice versa.

In the case of the second layer, the Wenner β array has the smallest absolute error at 12.80 Ωm, while the Wenner α and γ arrays have values of 16.89 Ωm and 17.95 Ωm, respectively. Since the high resistivity substratum is first observed on the array with the greatest depth of investigation, the Wenner γ array now has the highest mean resistivity.

In the third layer case, the Wenner γ array with the lowest *ABSE* values was closest for determining the true substratum resistivity. Because the *ABSE* values are calculated based on the mean apparent resistivity, the *ABSE* values are quite high; however, the

Table 2. Statistical summary for the three Wenner arrays and the three layers of the model; ρ_{min} −minimal resistivity; ρ_{max} − maximal resistivity; ρ_{mean} − mean resistivity; ABSE – absolute error.

Array	Name	Layer 1				Layer 2				Layer 3			
		ρ_{min} [Ωm]	ρ_{max} [Ωm]	ρ_{mean} [Ωm]	ABSE [Ωm]	ρ_{min} [Ωm]	ρ_{max} [Ωm]	ρ_{mean} [Ωm]	ABSE [Ωm]	ρ_{min} [Ωm]	ρ_{max} [Ωm]	ρ_{mean} [Ωm]	ABSE [Ωm]
Wenner Alpha	M1	90.04	113.44	102.35	2.35	6.18	51.96	16.60	6.60	20.17	578.79	120.70	379.30
	M2	67.23	131.16	97.34	2.66	7.54	43.97	15.89	5.89	8.85	694.79	95.94	404.06
	M3	53.47	133.11	93.18	6.82	10.71	36.33	17.68	7.68	10.71	567.16	64.05	435.95
	M4	70.83	126.62	102.24	2.24	14.26	60.06	28.18	18.18	14.26	495.09	51.65	448.35
	M5	39.66	133.33	89.33	10.67	18.24	41.32	27.93	17.93	18.24	502.45	48.58	451.42
	M6	41.82	121.56	88.28	11.72	25.46	42.72	35.12	25.12	24.68	391.51	53.66	446.34
	M7	50.16	122.51	88.47	11.53	42.57	51.15	46.82	36.82	37.62	382.71	70.55	429.45
	Average	59.03	125.96	94.46	6.85	17.85	46.79	26.89	16.89	19.22	516.07	72.16	427.84
Wenner Beta	M1	96.76	115.85	105.36	5.36	5.95	48.27	16.17	6.17	30.83	325.67	107.52	392.48
	M2	66.54	137.87	97.69	2.31	7.25	41.98	15.08	5.08	21.09	487.50	110.70	389.30
	M3	52.21	127.06	92.56	7.44	8.74	38.50	16.91	6.91	12.93	414.57	85.87	414.13
	M4	49.82	122.49	91.06	8.94	10.83	35.69	19.21	9.21	11.83	317.50	64.48	435.52
	M5	41.18	126.71	90.88	9.12	12.95	36.84	22.01	12.01	13.56	302.99	54.19	445.81
	M6	60.51	128.53	98.16	1.84	18.45	52.26	32.54	22.54	18.45	210.04	52.21	447.79
	M7	50.17	131.37	96.46	3.54	26.20	52.59	37.69	27.69	26.20	230.85	64.88	435.12
	Average	59.60	127.13	96.02	5.51	12.91	43.73	22.80	12.80	19.27	327.02	77.12	422.88
Wenner Gamma	M1	98.99	113.42	105.00	5.00	6.41	50.86	17.19	7.19	31.65	704.80	156.50	343.50
	M2	70.48	133.22	98.96	1.04	8.36	45.12	16.77	6.77	17.88	1000.76	127.56	372.44
	M3	56.14	134.94	94.56	5.44	11.22	41.08	18.88	8.88	14.01	809.38	82.06	417.94
	M4	45.63	129.35	90.68	9.32	16.28	40.76	23.66	13.66	16.36	541.55	58.66	441.34
	M5	42.26	134.41	89.16	10.84	20.96	41.00	29.35	19.35	22.23	438.36	54.48	445.52
	M6	43.25	130.68	87.50	12.50	30.58	49.48	38.80	28.80	30.58	369.88	60.86	439.14
	M7	49.43	134.11	87.40	12.60	44.93	58.60	51.00	41.00	47.02	345.43	81.56	418.44
	Average	58.02	130.02	93.32	8.11	19.82	46.70	27.95	17.95	25.68	601.45	88.81	411.19

Wenner γ array exhibited the lowest *ABSE* values and the highest mean resistivity values with 88.81 Ωm, as well as the highest maximal resistivity in the third layer with the average maximal resistivity value at around 600 Ωm.

Using the data from the inverted models, a further statistical parameter was calculated. The coefficient of variation (*CV*) is a measure of data dispersion derived from the ratio of the standard deviation to the mean. The *CV* values for the three Wenner arrays on all three layers are displayed in Tab. 3.

The *CV* value for the first layer is the lowest on average among the three arrays, ranging from 18.78% to 21.8%. The *CV* value increases as the layers progress, reaching a maximum between 90% and 110% for the third layer. It should also be noted that the *CV* values for the second layer exhibit a decreasing trend, whereas the trends for the first and third layers are different. Consequently, Pearson's and Spearman's correlation coefficients could be utilized to conduct a correlation analysis between the parameters of the

Table 3. Coefficient of variation (CV) values for the three Wenner arrays and all the three layers of the model.

Array	Name	Layer 1 CV [%]	Layer 2 CV [%]	Layer 3 CV [%]
Wenner Alpha	M1	3.83	78.50	87.29
	M2	20.44	64.02	116.08
	M3	26.17	44.19	132.56
	M4	14.97	49.19	132.12
	M5	26.43	21.71	130.84
	M6	25.61	11.03	97.96
	M7	22.64	5.08	75.35
	Average	20.01	39.10	110.32
Wenner Beta	M1	4.31	74.26	70.29
	M2	21.87	60.18	90.81
	M3	24.47	53.06	109.08
	M4	23.80	42.41	106.56
	M5	23.40	31.77	103.61
	M6	15.04	31.80	83.19
	M7	18.60	20.74	72.95
	Average	18.78	44.89	90.93
Wenner Gamma	M1	3.11	75.03	87.33
	M2	19.47	60.23	119.33
	M3	24.53	44.26	134.32
	M4	27.76	28.18	120.81
	M5	28.06	18.03	103.76
	M6	25.97	11.81	80.05
	M7	23.74	5.59	59.50
	Average	21.80	34.73	100.73

*Table 4. Correlation of the thickness of the second layer (h_2) and the coefficient of variation (CV); r –
Pearson's correlation coefficient; r_s – Spearman's correlation coefficient.*

Correlation of h_2 and CV						
Array/parameter	Layer 1		Layer 2		Layer 3	
	r	r_s	r	r_s	r	r_s
Wenner Alpha	−0.63	−0.50	0.98	0.96	0.24	0.25
Wenner Beta	−0.30	0.00	0.98	0.96	0.06	0.04
Wenner Gamma	−0.69	−0.54	0.98	1.00	0.56	0.54
Legend (after Schober et al., 2018)						
Description	Color				Range	
Negliglible					0.0–0.1	
Weak					0.1–0.39	
Moderate					0.4–0.69	
Strong					0.7–0.89	
Very strong					0.9–1.0	

second layer thickness (h_2) and the CV. The correlation analysis can be seen in Tab. 4, where the correlation ranges from Schober et al. (2018) are used. For the first layer, the Wenner α and γ arrays exhibit a moderate, negative correlation, which indicates that as the thickness of the second layer decreases, the data dispersion (CV) increases. The Wenner β array yields contradictory results, as the Pearson correlation coefficient suggests a negative, weak correlation whereas the Spearman correlation coefficient suggests a nonexistent correlation. The second layer revealed a very strong correlation from all three Wenner arrays, *i.e.*, as the second layer's thickness decreases, so does the resistivity data dispersion. The results of the third layer are comparable to the average depth of investigation. The Wenner β array with the shallowest depth of investigation has negligible correlation between the second layer's thickness and data dispersion. In contrast, the array with the greatest depth of investigation has the strongest positive correlation with data dispersion in relation to the thickness of the second layer. When the thickness of the second layer is altered, the array with the greatest depth of investigation will have the largest data discrepancy of deeper layers.

The results presented here only illustrate one situation, in which resistivity decreases with depth, or the H-type curve if 1D resistivity sounding were performed. To provide a general recommendation for field surveys, additional modeling and statistical analysis are required in which various models with varying thicknesses are analyzed. In addition, modern survey techniques employing multicore cables enable relatively rapid data acquisition with various arrays. Due to this, all three Wenner arrays can be acquired with relative ease, where electrode switching is performed by a field computer and no additional effort is required by field technicians when switching from the Wenner α to the β or γ arrays. Additional models are not presented in this research paper, but the equivalence case illustrated by the modified Ackworth and Griffits (1985) model should be the focus of future research.

3.2. Lateral effects and 1D inversion

It is obvious from the theoretically determined sounding curves ($\rho_a{}^\alpha$, $\rho_a{}^\beta$, and $\rho_a{}^\gamma$) that there is no common general pattern in the presence of a vertical contact between two mediums of different resistivities. However, the sounding curves are better described by mutual convergence and divergence. The sounding curve for $\rho_a{}^\beta$ diverges from the $\rho_a{}^\alpha$ and $\rho_a{}^\gamma$ sounding curves, which are mutually comparable (Fig. 5a).
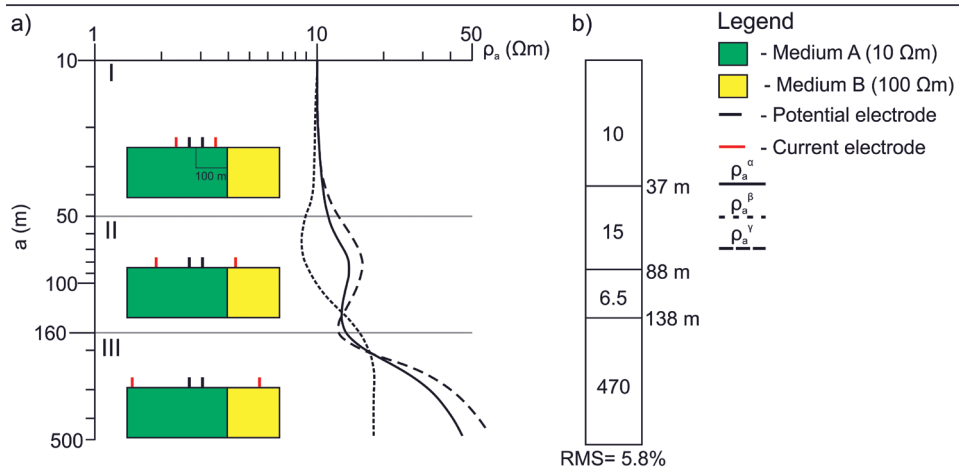
Figure 5. (*a*) Sounding curves of Wenner α, β and γ array over a vertical contact; (*b*) 1D inversion of the $\rho_a{}^\alpha$ sounding curve; ρ_a – apparent resistivity.

The additional sounding curves $\rho_a{}^\beta$ and $\rho_a{}^\gamma$ allow for the identification of lateral effects that are primarily bound to the current electrode, which is not possible with normal-sounding methodology. Figure 5a shows the divergence of the sounding curves $\rho_a{}^\alpha$, $\rho_a{}^\beta$ and $\rho_a{}^\gamma$ as the current electrode approaches the vertical contact. The same divergence can also be seen as the current electrode transitions into the second medium with a higher resistivity value (segment I and II in Fig. 5a). The lateral effect could only be detected using the $\rho_a{}^\alpha$ sounding curve with the electrode spacing (a) greater than 160 m and when the potential electrode moves into the second medium. Only the slope of the last segment of the $\rho_a{}^\alpha$ sounding curve could suggest a vertical contact. The rest of the diagram could be interpreted as the sounding curve over a horizontally layered subsurface. Quantitative 1D inversion, which would be performed after smoothing of the $\rho_a{}^\alpha$ sounding curve, would result in an erroneous four-layer subsurface model (Fig. 5b). The last section of the $\rho_a{}^\alpha$ sounding curve is responsible for the higher root-mean-square (*RMS*) value of around 5.8%.

Aside from qualitative analysis of the data, quantitative determination of lateral effects is feasible. If the lateral effects are not overly articulated, a numerical adaptation of the data to a 1D subsurface model is possible. The lateral effect is quantified using a numerical approach proposed by Habberjam and Watkins (1967a) calculating the lateral inhomogeneity ratio (*LIR*) and the index of lateral inhomogeneity (*LII*).

Figure 6a shows the effects of geoelectrical sounding processing in Vrdnik (Serbia) using the Wenner tri-potential technique. Vrdnik is located in northern Serbia on the southern slope of the Fruška gora mountain. The geology of the Vrdnik locality consists of Miocene limestones, sandstones, conglomerates as well as freshwater lacustrine coal beds, while the uppermost layers are composed of Quaternary gravel, sands, and Pleistocene loess (Čičulić-Trifunović and Rakić, 1971). The example shows an increase in processing covariance as the index of lateral inhomogeneity rises.

The root-mean-square measurement accuracy value in the studied area is ±4%. This implies that the minimal expected processing covariance value should be 0.0003 in the case of a 1D subsurface model. Any deviation of the local geology from a 1D model will lead to the increase of processing covariance. With values of the lateral inhomogeneity index of 110% (Fig. 6a), the processing covariance is 0.092 confirming that the 1D inversion of sounding data is inadequate.

The value of processing covariance is significantly lower in Golubac (Serbia) (Figure 6b). Golubac is situated on the border between Serbia and Romania on the right bank of the Danube River (eastern Serbia). The sediments of the Golubac locality are comprised of middle Miocene sands, sandstones, conglomerates, and gravelly alluvium (Kalenić et al., 1973).

The measurements were carried out with the square array since the square array is less sensitive to lateral effects than colinear arrays (Habberjam, 1972a; Sretenović et al.,
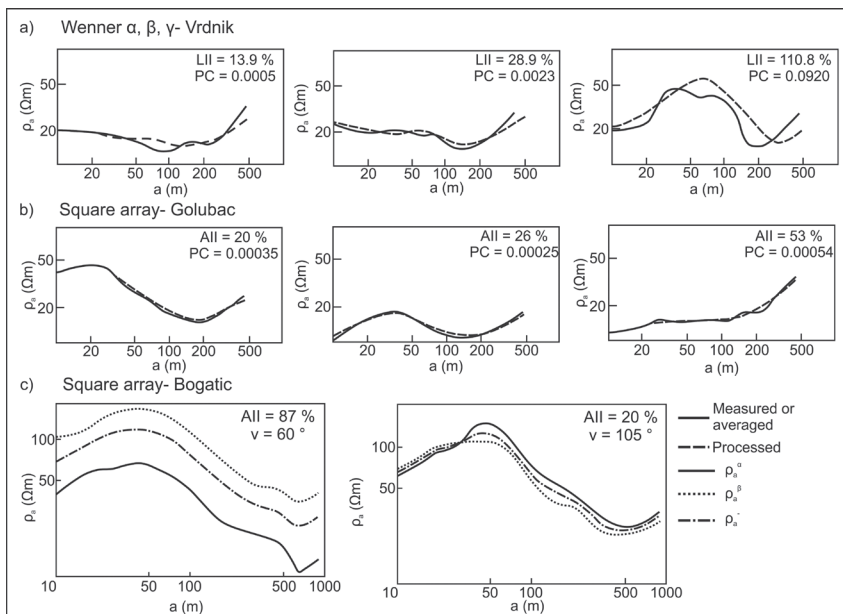

Figure 6. (*a*) Geoelectrical processing results with the Wenner tri-potential technique in Vrdnik (Serbia); (*b*) Geoelectrical processing results with the square array in Golubac (Serbia); (*c*) Geoelectrical sounding curve in Bogatić (Serbia) with two different square array orientations; ρ_a – apparent resistivity.

2014; Udosen and George, 2018; Sretenović and Arnaut, 2019). By averaging the $\rho_a{}^\alpha$ and $\rho_a{}^\beta$ sounding curves, local near-surface inhomogeneities are reduced. The averaged sounding curve $\rho_a{}^{ave}$ is of higher quality than sounding curves obtained with colinear electrode arrays. The processed sounding curve $\rho_0{}^o$ is adapted to the conditions of a horizontally layered subsurface. Lower processing covariance values are a function of the numerical method for lateral effects reduction being based on the use of the square array, while the Wenner array requires two sub-arrays (α and γ).

Figure 6b shows the results of the square array geoelectrical sounding processing in Golubac. The processed sounding curves show that they are more adapted to the 1D horizontally layered subsurface half-space than data obtained using the Wenner tri-potential technique. The processing covariance is used to compare the results of the two arrays. The distinct differences between the $\rho_a{}^\alpha$ and $\rho_a{}^\beta$ sounding curves are mirrored by high values of azimuthal inhomogeneity index (*AII*). The differences could be the result of anisotropy or deeper 2D structures. Regardless of the relatively low processing covariance values, interpretation with the 1D model assumption can be inadequate in both cases. In that case, further investigations with the crossed square array are required.

Because both the ratio and index of azimuthal inhomogeneity are dependent on the orientation of the square array relative to the subsurface strike or electrical anisotropy, low values of the *AII* do not guarantee that the subsurface is horizontally layered, which was supported by the Bogatić field example (Fig. 6c). Bogatić is situated in western Serbia, and its geology consists primarily of fluvial structures formed by the accumulation of sediments from the rivers Drina and Sava. The accumulated river terrace sediments have a relative thickness of 3 to 10 meters and are primarily composed of sandy gravel, gravel, siltstones, and sandstones which was deposited during the late Pleistocene and early Holocene. Deeper levels mainly consist of sands, silty sands, and clays. (Rajčević, 1978; Vrhovčić et al., 1986).

Both *AIR* and *AII* are theoretically equal to zero when the square array orientation relative to electrical strike is 45 degrees. This implies that the presence of a structure or electrical anisotropy will not be detected (Habberjam, 1975). The averaged sounding curve from four directions (ρ_x) is independent of the array orientation (Habberjam and Watkins, 1967b; Habberjam, 1972b; Habberjam and Jackson, 1974), and it reduces lateral effects by averaging apparent resistivity data from four directions. After analyzing electrical anisotropy using the crossed square array the mean apparent resistivity sounding curve (ρ_m) can be calculated. The ρ_m sounding curve is orientationally independent of the square array orientation but takes into consideration the effects of electrical anisotropy (Habberjam and Watkins, 1967b).

The Wenner tri-potential array cannot differentiate local 2D and 3D near-surface inhomogeneities from the effect of deeper 2D structures during lateral effects detection, quantification, and reduction. This unavoidable noise can be reduced during the measurement phase, but not during the phase of numerical processing (Barker, 1981; Barker, 1989). Because of the need for more efficient data acquisition (just half of the points on the sounding curve are measured while the rest are calculated), this technique was not chosen.

The offset Wenner array was used to perform an experimental survey. The survey included measuring resistances $R_1{}^\alpha$ and $R_2{}^\alpha$ in every data point of the apparent resistivity sounding curve, and then comparing measured and theoretically calculated apparent resistivity values using Barker's method (1981). Horizontal stratification was expected on the Zemun loess plateau, where the survey was conducted. The Zemun loess plateau
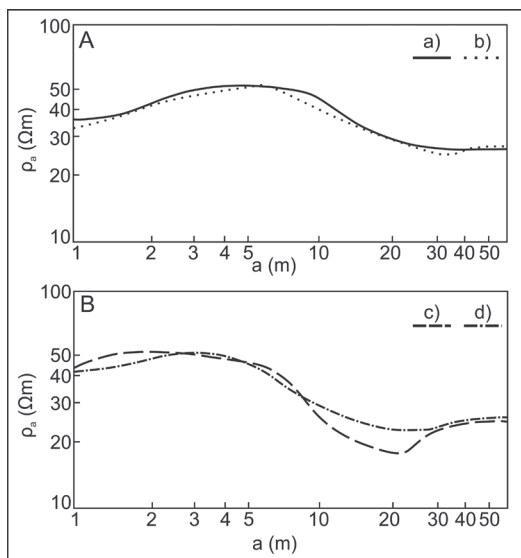
Figure 7. Sounding sites *A* and *B* during the verification of the offset Wenner array; a, b, c, and d – sounding curves; ρ_a – apparent resistivity.

is located in the Zemun municipality of Belgrade (Serbia) and consists of yellow, upper Pleistocene, sandy-clayey siltstones that formed during glacial periods (Marković et al., 1984). With that kind of local geology, the combined influence of deeper structures and local near surface inhomogeneities were avoided. To determine the subsurface architecture, sounding was carried out at two sounding sites, each with two perpendicular measurements. If the conditions of a 1D model are true, and there are no significant deviations of apparent resistivity sounding curves in both directions, the values of E_{of} can be related to local near-surface lateral inhomogeneities. Figure 7 displays the sounding curves R_1^{α} and R_2^{α} in both sounding sites with perpendicular measurements.

For sounding curves a, b, and d, the measured *RMS* values for E_{of} are around 6–10%, while the value for sounding curve c is around 35%. Since c is the sounding curve with the greatest lateral impact, the largest discrepancy between theoretically calculated and measured values is probable. Table 5 shows the previously mentioned divergences, as well as E_{inter} (interpolation error) and E_{extr} (extrapolation error).

Table 5. Estimated RMS values E_{of} and discrepancies between measured and theoretically calculated apparent resistivity values; E_{of} – offset error, E_{inter} – interpolation error, E_{extr} – extrapolation error; a, b, c, and d – sounding curves.

RMS/Sounding curve	a	b	c	d
E_{of} [%]	9.7	10.3	34.8	6.4
E_{inter} [%]	6.5	6.8	17.9	7.3
E_{extr} [%]	35.3	27	94.4	32.7

The highest values of discrepancy are determined for the sounding curve c which is the curve with the most lateral impact. For sounding curves, a, b, and d, the root-mean-square value E_{inter} is around 6.5%–7.5%, whereas, for diagram c, the value is around 18%. Extrapolation error (E_{extr}) *RMS* values are much larger, varying from 27% to 94%, which is unacceptable when measuring the extrapolated apparent resistivity value based on a twofold smaller value of a. Significantly higher E_{extr} values can not be explained solely by lateral effects that are insignificant on sounding curves a, b, and d. Furthermore, theoretically calculated extrapolated values of apparent resistivity show a significant difference from measured results. The reason for this is that the estimation of electrical resistance $R_a(2a)$ is based on the measurement of electrical resistances $R_a(a)$ and $R_c(a)$ (Eq. (9)), which can be nearly equivalent in the case of very small $R_a(2a)$. Calculating $R_a(2a)$ from $R_a(a)$ and $R_c(a)$ values that are nearly identical and very small will result in error magnification. When the apparent resistivity sounding curve is descending, the problem is more pronounced. However, when the apparent resistivity sounding curve is ascending and the difference between $R_a(a)$ and $R_c(a)$ is distinct, the problem is less pronounced.

$$R_a(2a) = 2[R_c(a) - R_a(a)]. \tag{9}$$

Discrepancies E_{inter} are primarily caused by lateral inhomogeneities near the surface. With larger electrode spacing (a) can lead to higher error values when measuring $R_b(a)$ and $R_b(2a)$ due to dipole-dipole array measurements ($C_1C_2P_1P_2$), where the electrical potential drops with the square of the distance, increasing the error when calculating the resistance $R_a(3a)$ (Eq. (10)).

$$R_a(2a) = 0.5R_a(2a) + R_b(2a) - R_b(a) + 0.5R_a(4a). \tag{10}$$

The sounding curve in Fig. 8d corresponds to the averaged sounding curve "a" in Fig. 8c. The measurements were done with the first (Wenner I) and second (Wenner II) array (α, β, and γ). The method of Habberjam and Watkins (1967a) is used to calculate lateral effects. The index of lateral inhomogeneities in measurements with the Wenner I array is 17.5%. The *LII* in measurements with the Wenner II array is 24.1%, confirming that the subsurface architecture closely resembles a 1D model. The *RMS* of the E_{of}, which is 9.7%, supports this model as well.

Figure 8d marks some of the lateral effects that are caused by the discrepancy from horizontal stratification. The *RMS* of a 1D inversion of the averaged ρ_a^{ave} sounding curve is 2%, implying that simple averaging is sufficient for lateral effects reduction (Fig. 8d).

3.3. 1D Lateral effects caused by 2D and 3D inhomogeneities

The development of fully automated 2D acquisition systems, which collect more resistivity data than conventional 1D survey systems, is attributable to the advancement of geoelectrical acquisition methodology. It was not possible to process large amounts of data in a short amount of time with 1D sounding methodology prior to the development of software packages such as the widely used RES2DINV. Due to this, 2D lateral effects can be easily displayed on models derived after inversion, yielding a more accurate depiction of the subsurface architecture than 1D surveys.

Figure 9a shows a horizontally layered subsurface model with 2D near-surface inhomogeneities. Sounding curves of apparent resistivity were calculated for that subsurface
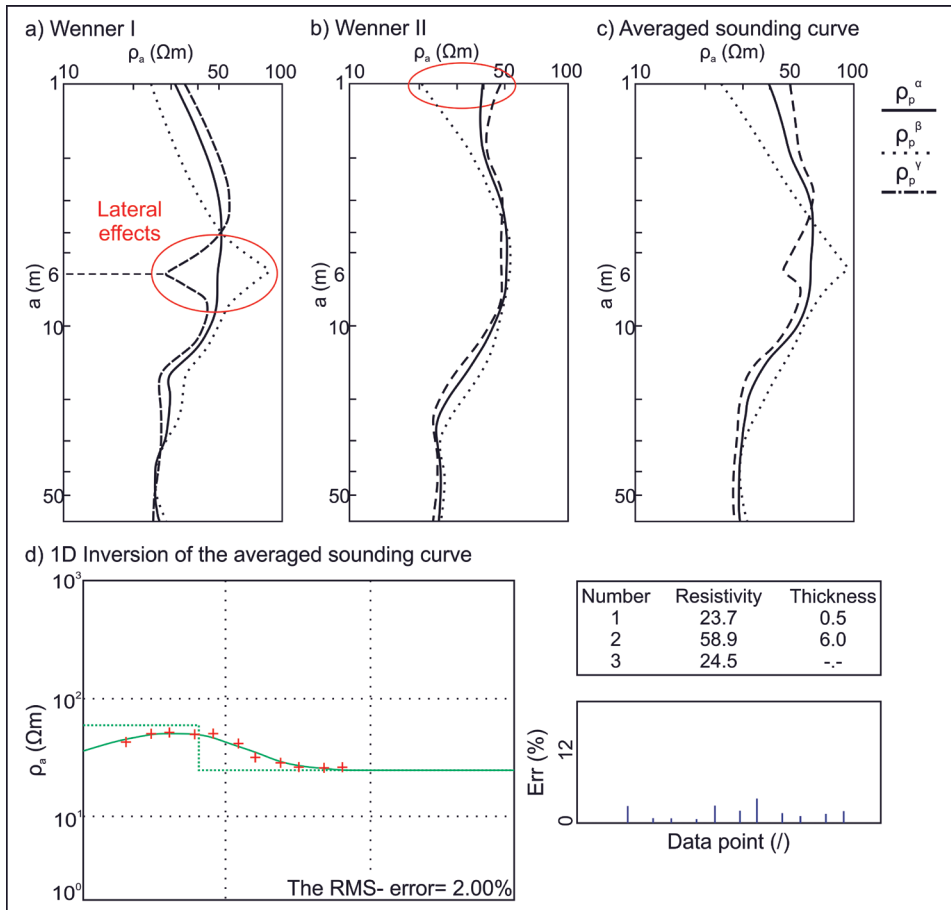
Figure 8. Sounding results with the offset Wenner array (Zemun loess plateu). Sounding curves α, β, and γ measured with (*a*) the Wenner I and (*b*) Wenner II array; (*c*) averaged sounding curves α, β, and γ from the measurements with the Wenner I and II array; (*d*) 1D inversion of the averaged sounding curve (Wenner I and II array averaged); ρ_a - apparent resistivity.

model using the offset Wenner array (α, β, and γ), as shown in Fig. 10. The lateral effects of 2D inhomogeneities that rise to the surface and are present at any depth level can be seen in sections of apparent resistivity. In the case of a 1D model, isolines of apparent resistivity should be horizontal. A distinct lateral effect was observed before the start of 2D inversion in RES2DINV. It was proposed that inversion be done with a cell size equal to half the size of the unit electrode spacing (a) in order to reduce the amount of lateral effects. The achieved *RMS* difference between observed and theoretically calculated data was 1.94%. Two additional parameters were applied:

1. vertical/horizontal flatness ration = 0.3 and,
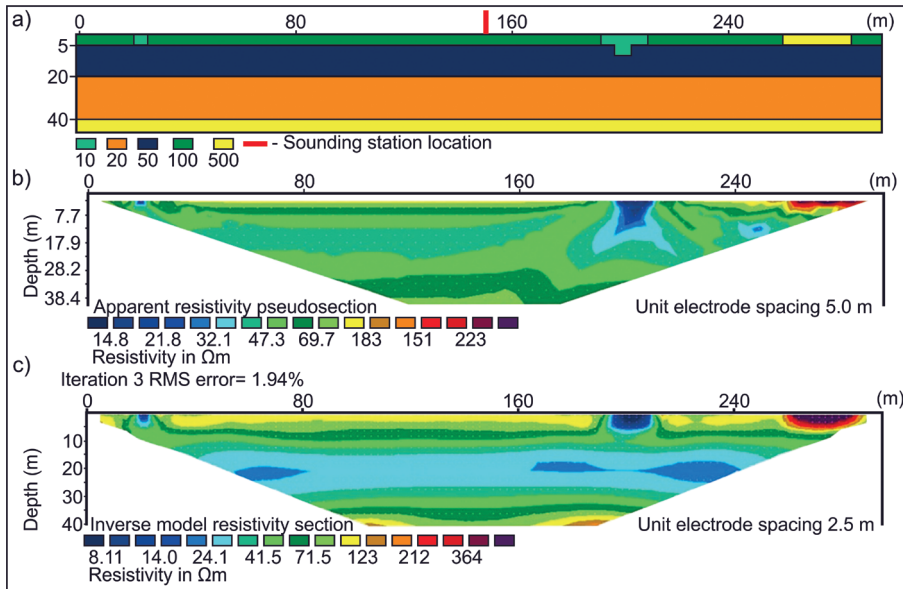2. increase of damping factor with depth =1.2.

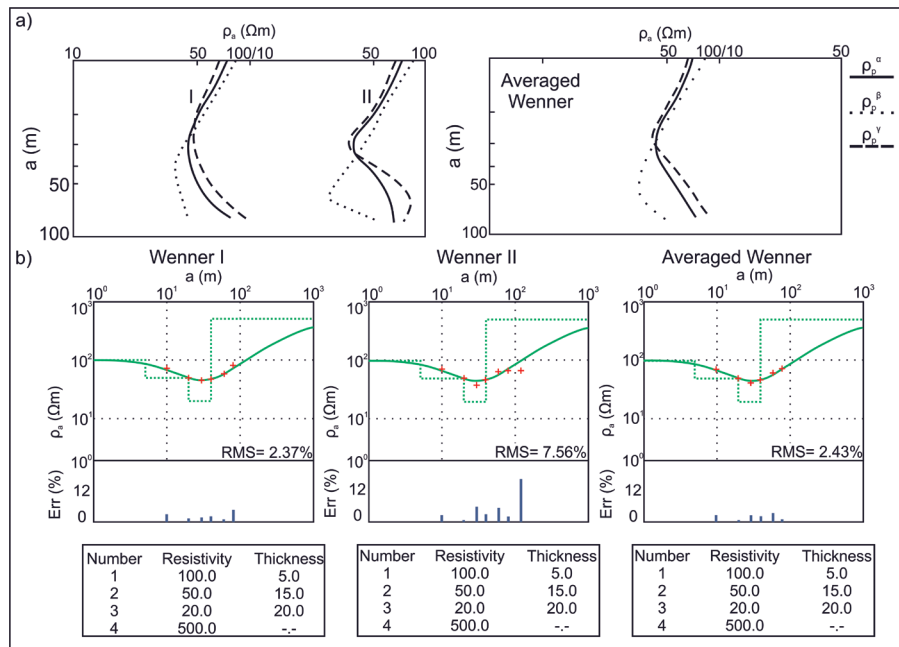**Figure 9.** (*a*) Subsurface model; (*b*) Section of apparent resistivity; (*c*) 2D inversion results.

Figure 10. (*a*) Offset Wenner sounding curve for the α, β, and γ array; (*b*) 1D inversion results of Wenner I, Wenner II and Wenner averaged sounding curve; ρ_a – apparent resistivity.

Figure 10a shows the sounding curves of the Wenner α, β, and γ array in the case of averaging the apparent resistivity sounding curves of Wenner I and Wenner II to obtain two sounding curves. The sounding curves ρ_a^{α}, ρ_a^{β}, and ρ_a^{γ}, which correspond to the I and II Wenner arrays, indicate different lateral impacts, which are later verified by processing results (*LII*= 2.6% and 6.2%, respectively). From a 1D inversion perspective, the *RMS* offset value of 10.85% closely resembles the 10% value that Barker (1981) suggests as good quality data. Figure 10b shows the discrepancies between apparent resistivity sounding curves calculated for the 1D subsurface without near-surface inhomogeneities and sounding curves with near-surface lateral inhomogeneities (Wenner I, Wenner II, and Wenner averaged). The sounding curve Wenner II has the greatest difference (*RMS* error = 7.6%), while the Wenner average and Wenner I data have a discrepancy of 2.4%. 1D inversion of the Wenner II array sounding curve did not create an *RMS* error of less than 5.5%.

Two boundary cases for detecting local 3D near-surface inhomogeneity (spherical shape) are shown in Fig. 11a. The apparent resistivity anomalies (α, β, and γ) cannot be observed when the depth to the sphere center (*H*) and the radius of the sphere (*R*) are approximately $H/R \geq 2$ and the geoelectrical profile passes through the projection of the center of the sphere to the surface (*B* = 0 m). This is because they do not reach the 10% threshold of the true resistivity of the surrounding material, in this case, 100 Ωm. This anomaly would be very small (around 5%) due to ambient noise and lateral effects from other near-surface inhomogeneities, so the sphere would not be detectable (Fig. 11a).
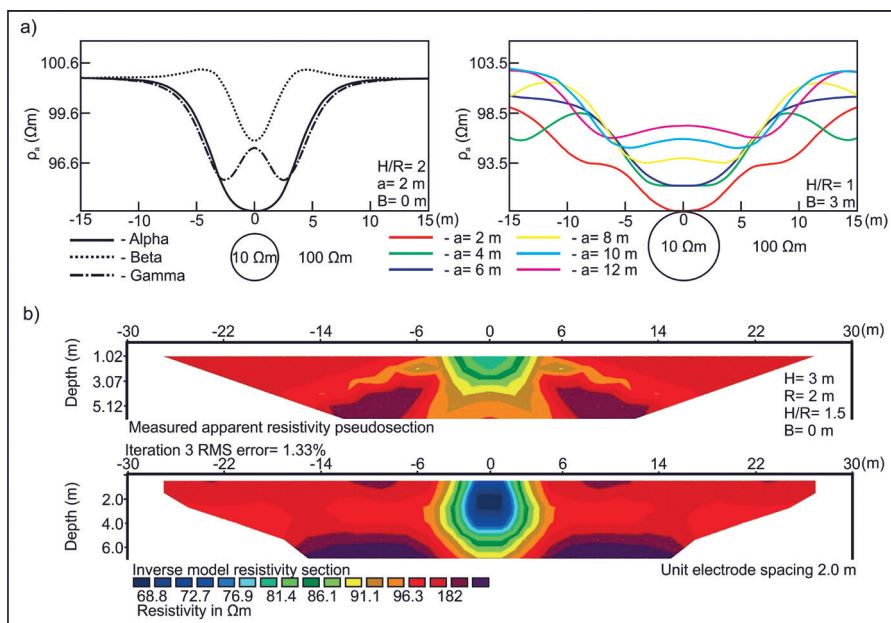

Figure 11. (*a*) Boundary cases during the detection of a spherical inhomogeneity (a) $H/R \geq 2$, (b) $H/R = 1$; (*b*) 2D survey over a spherical inhomogeneity section of apparent resistivity and a 2D inversion result; ρ_a – apparent resistivity.

The second boundary case is a spherical inhomogeneity that emerges to the surface ($H/R = 1$) when the detectability is certain. Anomaly intensity of a sphere is dependent on the Wenner electrode array separation (a) and the radius of the sphere (R). As a result, sounding curves for six depth levels were calculated, beginning with the smallest electrode spacing of $a_{min} = 2$ m and rising to $a_{max} = 12$ m. Figure 11a indicates that the anomaly intensity decreases as the ratio a/R increases. Since using larger measurements of the Wenner electrode array results in a higher impact of true resistivity of the environment (100 Ωm) compared to the apparent resistivity.
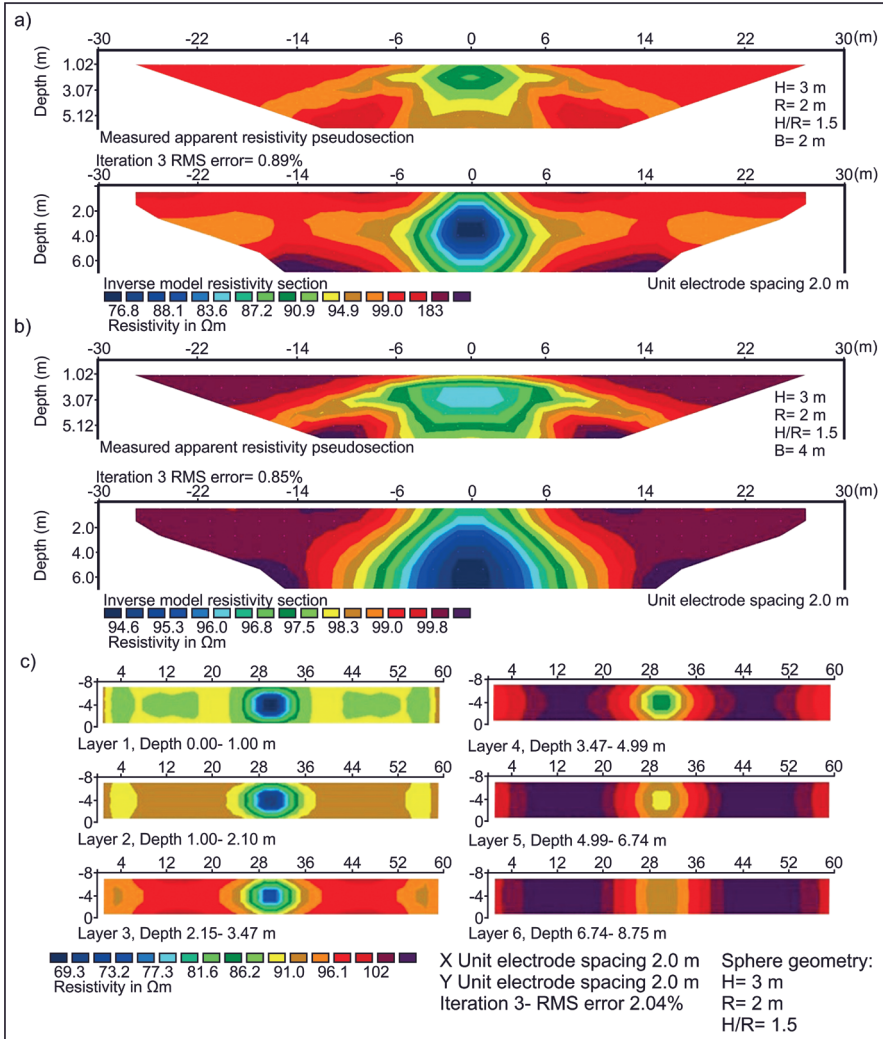

Figure 12. 2D survey over a spherical inhomogeneity. 2D profile with a shift of 2 m (*a*) and 4 m (*b*) from the projection of the sphere's center to the surface; (*c*) Conversion of 2D profiles to 3D format.

Figure 11b shows a 2D survey (ERT) over a spherical 3D near-surface inhomogeneity with a depth of $H = 3$ m and a radius of $R = 2$ m. The profile line passes through the center of the sphere's surface projection ($B = 0$ m). The existence of lateral effects that are symmetrically spread from the anomaly and distributed in all directions can be seen in the apparent resistivity section (Fig. 11b). The 2D inverse model shows an accurate depth to the center of the sphere as well as its radius, but not an accurate approximation of the true resistivity (60 Ωm instead of 10 Ωm). That effect is understandable provided that the anomaly from the sphere decreases rapidly as the ratio H/R (in this case $H/R = 1.5$).

Figures 12a and 12b show a two-dimensional ERT survey with a lateral shift from the sphere's projection to the surface ($B = 2$ m and $B = 4$ m). The anomalies caused by the existence of a 3D inhomogeneity (in this case a sphere) easily become undetectable.

The results of converting a 2D profile set to pseudo or semi 3D are shown in Fig. 12c. The position of the sphere is detectable (x, y, and z coordinates) in the first three layers (depth from 0 to 3.5 m), but the true resistivity is overestimated (70 Ωm instead of 10 Ωm). The last three layers (depths of 3.5 m to 8.75 m) steadily decrease true resistivity intensity and the sphere shape, which corresponds to the decrease in anomaly intensity induced by the sphere.

4. Conclusion

Resistivity surveys using the Wenner tri-potential technique, Offset Wenner, and the square array were presented to identify, quantify, and reduce lateral effects, as well as to narrow the equivalence range for various surveys in Serbia.

Model equivalence analysis revealed that the Wenner β array provides the best results for the first and second layer resistivities, whereas the Wenner γ array provides the highest apparent resistivity values and the lowest *ABSE* value for the third, highly resistive layer.

By averaging the electrical resistance values ($R_1{}^\alpha$ and $R_2{}^\alpha$), it is possible to obtain an apparent resistivity sounding curve that is relatively free of lateral effects caused by 2D and 3D near-surface inhomogeneities. By averaging the values of all measured electrical resistances with the Offset Wenner array lateral effects reduction of local near surface inhomogeneities is achieved. In addition, the method developed by Habberjam and Watkins (1967b) permits a quantitative approximation and reduction based on these averaged values. A field investigation in the Zemun loess plateau demonstrates this possibility.

The Wenner tri-potential technique was applied in the Vrdnik survey (Serbia) where the *LII* values of 110% and the *PC* values of 0.092 confirmed that the 1D inversion was inadequate. In contrast, the *PC* values were lower in Golubac (Serbia), where the square array survey was applied. Because square array is less sensitive to lateral effects than collinear arrays, the averaged sounding curve was of higher quality than the sounding curves obtained from collinear arrays. When the 1D interpretation is inadequate due to electrical anisotropy or the effects of deeper structures, as reflected by high *AII* values, the crossed square array must be used to conduct additional research.

The Offset Wenner array was utilized to validate the interpolated and extrapolated values. It was determined that the interpolated apparent resistivity values were reasonably accurate. Extrapolated values are inadequate when resistivity decreases with depth, *i.e.*, when a low-resistivity substratum exists.

Due to the length of the paper, the equivalence scenario was not fully explored; ongoing research focuses exclusively on the equivalence principle with a two-layer starting model. This will enable better characterization of the depth of detectability and the possible narrowing of the equivalence range with different arrays.

References

Acworth, R. I. and Griffiths, D. H. (1985): Simple data processing of tripotential apparent resistivity measurements as an aid to the interpretation of subsurface structure, *Geophys. Prospect.*, **33**, 861–887, https://doi.org/10.1111/j.1365-2478.1985.tb00782.x.

Barker, R. D. (1989): Comment on "Examination of sounding curve extrapolation used by the offset wenner system" by White, P. A. and Scott, D. M., *Geophys. Prospect.*, **37**, 107–110, https://doi.org/10.1111/j.1365-2478.1989.tb01824.x.

Barker, R. (1981): The offset system of electrical resistivity sounding and its use with a multicore cable, *Geophys. Prospect.*, **29**, 128–143, https://doi.org/10.1111/j.1365-2478.1981.tb01015.x.

Bhattacharya, B. B. and Shalivahan, S. (2016): *Geoelectric methods: Theory and application.* McGraw Hill Education (India).

Bhattacharya, P. K. and Patra, H. P. (1968): *Direct current geoelectric sounding: Principles and interpretation.* Elsevier Publishing Company.

Busby, J. P. and Peart, R. J. (1997): Azimuthal resistivity and seismic measurements for the determination of fracture orientations, *Eng. Geol. Spec. Pub.,* Geological Society, London, **12**, 273–281, https://doi.org/10.1144/GSL.ENG.1997.012.01.24.

Carpenter, E. W. and Habberjam, G. M. (1956): A tri-potential method of resistivity prospecting, *Geophys.,* **21**, 455–469, https://doi.org/10.1190/1.1438247.

Carpenter, E. W. (1955): Some notes concerning the Wenner configuration, *Geophys. Prospect.*, **3**, 388–402, https://doi.org/10.1111/j.1365-2478.1955.tb01384.x.

Chermali, M., Bellalem, F., Belgroun, M. W., Boudella, A. and Bounif, M. O. (2018): Examination of the validity of the computed intermediate apparent resistivity points in the Wenner and offset Wenner configuration of sounding, *Acta Geod. Geophys.,* **53**, 661–677, https://doi.org/10.1007/s40328-018-0236-x.

Čičulić-Trifunović, M. and Rakić, M. O. (1971): *Basic geologic map of Former Yugoslavia 1:100 000, Explanatory booklet for the Sheet of Novi Sad.* Federal Geological Survey, Belgrade (in Serbian).

Edwards, L. S. (1977): A modified pseudosection for resistivity and IP, *Geophys.*, **42**, 1020–1036, https://doi.org/10.1190/1.1440762.

Habberjam, G. M. (1975): Apparent resistivity, anisotropy and strike measurements, *Geophys. Prospect.*, **23**, 211–247, https://doi.org/10.1111/j.1365-2478.1975.tb01525.x.

Habberjam, G. M. and Jackson, A. A. (1974): A resistivity section of Holy Island (Anglesey), *Geol. J.,* **9**, 167–174, https://doi.org/10.1002/gj.3350090205.

Habberjam, G. M. (1972a): The effects of anisotropy on square array resistivity measurements, *Geophys. Prospect.*, **20**, 249–266, https://doi.org/10.1111/j.1365-2478.1972.tb00631.x.

Habberjam, G. M. (1972b): The point of assignment of an earth-resistance measurement, *Geoexpl.,* **10**, 141-148, https://doi.org/10.1016/0016-7142(72)90029-4.

Habberjam. G. M. (1969): The location of spherical cavities using a tripotential resistivity technique, *Geophys.* **34**, 780–784. https://doi.org/10.1190/1.1440049.

Habberjam, G. M. and Watkins, G. E. (1967a): The use of a square configuration in resistivity prospecting, *Geophys. Prospect.,* **15**, 445–467, https://doi.org/10.1111/j.1365-2478.1967.tb01798.x.

Habberjam, G. M. and Watkins, G. E. (1967b): The reduction of lateral effects in resistivity probing, *Geophys. Prospect.*, **15**, 221–235, https://doi.org/10.1111/j.1365-2478.1967.tb01785.x.

Kalenić, M., Hadži-Vuković, M., Dolić, D., Lončarević, Č. and Rakić, M. O. (1973): *Basic geologic map of Former Yugoslavia 1:100 000, Explanatory booklet for the Sheet of Kučevo*. Federeal Geological Survey, Belgrade (in Serbian).

Koefoed, O. (1969): An analysis of equivalence in resistivity sounding, *Geophys. Prospect.*, **17**, 327–335, https://doi.org/10.1111/j.1365-2478.1969.tb02087.x.

Loke, M. H. (2022): Tutorial: 2-D and 3-D electrical imaging surveys. Unpublished course notes (available at: https://www.geotomosoft.com/downloads.php).

Loke, M. H. (2016): RES2DMOD ver. 3.03. Rapid 2D resistivity forward modelling using the finite difference and finite-element methods. Wenner (alpha, beta, gamma), inline & equatorial dipole-dipole, pole- pole, pole- dipole and Wenner- Schlumberger. Freeware courtesy of M. H. Loke (available from https://www.geotomosoft.com/downloads.php).

Loke, M. H. (1994): The inversion of two-dimensional apparent resistivity data. Unpubl. Ph.D. thesis, University of Birmingham, U.K.

Maillet, R. (1947): The fundamental equations of electrical prospecting, *Geophys.*, **12**, 529–556, https://doi.org/10.1190/1.1437342.

Marković, B., Veselinović, M., Anđelković, J., Stevanović, P., Roglić, Č. and Obradinović, Z. (1984): *Basic geologic map of Former Yugoslavia 1:100 000, Explanatory booklet for the Sheet of Belgrade*. Federal Geological Survey, Belgrade (In Serbian).

Nunn, K. R., Barker, R. D. and Bamford D. (1983): In situ seismic and electrical measurements of fracture anisotropy in the Lincolnshire Chalk, *Q. J. Eng. Geol. Hydrogeol.*, **16**, 187–198, https://doi.org/10.1144/GSL.QJEG.1983.016.03.03.

Rajčević, D. (1978): *Basic Geologic Map of Former Yugoslavia 1:100 000, Explanatory booklet for the Sheet of* Šabac Federal Geological Survey, Belgrade (in Serbian).

Sanuade, O. A., Amosun, J. O., Oyeyemi, K. D., Olaojo, A. A., Fagbemigun, T. S. and Faloyo, J. I. (2019): Analysis of principles of equivalence and suppression in resistivity sounding technique, *J. Phys: Conf. Ser.*, 1299, https://doi.org/10.1088/1742-6596/1299/1/012065.

Schober, P., Boer, C. and Schwarte, L. A. (2018): Correlation coefficients: appropriate use and interpretation, *Anesth. Analg.,* **126**, 1763–1768, https://doi.org/10.1213/ANE.0000000000002864.

Sretenović, B. and Arnaut, F. (2019): Inadequacy of 1D, 2D and 3D resistivity inverse modeling in the presence of electrical anisotropy, *J. Earth. Sci.,* **8**, 102–116, https://doi.org/10.11648/j.earth.20190802.14.

Sretenović, B. B., Vasiljević, I. M. and Cvetkov, V. V. (2014): The application of geoelectrical attributes based on crossed square array resistivity sounding data at 'Pudarske Kolibe' site in eastern Serbia, *Teh.*, **69,** 604–609, https://doi.org/10.5937/tehnika1404604S.

Szalai, S., Lemperger, I., Metwaly, M., Kis, A., Wesztergom, V., Szokoli, K. and Novák, A. (2014): Multiplication of the depth of detectability using γ_{11n} arrays, *Appl. Geophys.,* **107**, 195–206, https://doi.org/10.1016/j.jappgeo.2014.06.003.

Szalai, S. and Szarka, L. (2008): On the classification of surface geoelectric arrays, *Geophys. Prospect.,* **56**, 159–175, https://doi.org/10.1111/j.1365-2478.2007.00673.x.

Udosen, N. I. and George, N. J. (2018): Characterization of electrical anisotropy in North Yorkshire, England using square arrays and electrical resistivity tomography, *Geomech. Geophys. Geo-energ. Geo-resour.,* **4**, 215–233, https://doi.org/10.1007/s40948-018-0087-5.

Vrhovčić, J., Buzaljko, R., Mojićević, M., Prtoljan, B., Galovilć, I., Marković, B., Anđelković, J., Pavlović, Z. and Rajčević, D. (1986): Basic *Geologic Map of Former Yugoslavia 1:100 000, Explanatory booklet for the Sheet of Bijeljina*, Federeal Geological Survey, Belgrade (in Serbian).

White, P. A. and Scott, D. M. (1988): Examination of sounding curve extrapolation used by the offset Wenner system, *Geophys. Prospect.*, **36**, 194–200, https://doi.org/10.1111/j.1365-2478.1988.tb02159.x.

Zhou, B. (2016): Electrical resistivity tomography: A subsurface-imaging technique, in: *Applied geophysics with case studies on environmental, exploration and engineering geophysics*, edited by Kanlı, A. I. IntechOpen, London, https://doi.org/10.5772/intechopen.81511.

Zohdy, A. A. (1949): Use of Dar Zarrouk curves in the interpretation of vertical electrical sounding data, *Geol. Surv. Bullet. 1313-D*, US Department of the Interior, Geological Survey, Washington, DC, https://doi.org/10.3133/b1313D.

SAŽETAK

Poboljšanje 1D geoelektričnog sondiranja sužavanjem raspona ekvivalencije i indentifikacija, kvantifikacija i redukcija lateralnih efekata korišćenjem tri-potencijalne metodologije

Filip Arnaut, Branislav Sretenović i Vesna Cvetkov

Podaci o prividnoj specifičnoj električnoj otpornosti prikupljeni Offset-Wenner dispozitivom (Zemun, Srbija), kvadratnim dispozitivom (Bogatić i Golubac, Srbija) i Wenner tri-potencijalnom metodologijom (Vrdnik, Srbija) korišteni su za detekciju, mjerenje i smanjenje bočnih nuspojava tijekom 1D inverzije. Direktno i inverzno modeliranjem s Wenner α, β i γ dispozitivima pokazalo je da Wenner β dispozitiv daje najbolju procjenu specifične električne otpornosti prvog i drugog sloja, dok je Wenner γ dispozitiv dao najbolju procjenu trećeg sloja, visokootpornog substratuma. Istraživanja na Zemunskom lesnom platou pokazala su da kada je indeks bočne nehomogenosti (*LII*) nizak, opravdana je 1D interpretacija oba Wenner dispozitiva. Također, usrednjavanje otpora će proizvesti krivulju otpora koja je oslobođena bočnih učinaka od blisko površinskih nehomogenosti. Da je 1D inverzija neadekvatna kada su *LII* i vrijednosti kovarijance procesinga (*PC*) velike prikazano je na primjeru Vrdnika. Primenom kvadratnog dispozitiva na lokalitetu Golubac dobijene su niže vrednosti *PC* od kolinearnih dispozitiva. Stoga je kvalitet osrednjene krivulje sondiranja bila veća. Interpolirane vrijednosti Offset-Wenner dispozitiva imale su dovoljnu preciznost, dok su ekstrapolirane vrijednosti bile neadekvatne u prisutnosti niskootpornog substratuma.

Ključne riječi: blisko-površinska ispitivanja, 2D geoelektrična tomografija, inverzija, Offset Wenner dispozitiv, kvadratni dispozitiv, efekti blisko-površinskih nehomogenosti na 1D ispitivanja

Corresponding author's address: Filip Arnaut, Department of Geophysics, Faculty of Mining and Geology, University of Belgrade, Đušina 7, 11120 Belgrade, Serbia; tel: +381 63 83 89 237; e-mail: filip.arnaut@rgf.rs